



THE UNIVERSITY *of* EDINBURGH

Edinburgh Research Explorer

## Mid-Level Dry Air Intrusions over the southern Maritime Continent

**Citation for published version:**

Aslam, A, Schwendike, J, Peatman, S, Birch, C, Bollasina, M & Barrett, P 2023, 'Mid-Level Dry Air Intrusions over the southern Maritime Continent', *Quarterly Journal of the Royal Meteorological Society*.  
<https://doi.org/10.1002/qj.4618>

**Digital Object Identifier (DOI):**

<https://doi.org/10.1002/qj.4618>

**Link:**

[Link to publication record in Edinburgh Research Explorer](#)

**Document Version:**

Peer reviewed version

**Published In:**

Quarterly Journal of the Royal Meteorological Society

**General rights**

Copyright for the publications made accessible via the Edinburgh Research Explorer is retained by the author(s) and / or other copyright owners and it is a condition of accessing these publications that users recognise and abide by the legal requirements associated with these rights.

**Take down policy**

The University of Edinburgh has made every reasonable effort to ensure that Edinburgh Research Explorer content complies with UK legislation. If you believe that the public display of this file breaches copyright please contact [openaccess@ed.ac.uk](mailto:openaccess@ed.ac.uk) providing details, and we will remove access to the work immediately and investigate your claim.



## ORIGINAL ARTICLE

# Mid-Level Dry Air Intrusions over the southern Maritime Continent

Ashar A. Aslam<sup>1</sup> | Juliane Schwendike<sup>1</sup> | Simon C. Peatman<sup>1</sup> | Cathryn E. Birch<sup>1</sup> | Massimo A. Bollasina<sup>2</sup> | Paul Barrett<sup>3</sup>

<sup>1</sup>School of Earth and Environment, University of Leeds, Leeds, LS2 9JT, UK

<sup>2</sup>School of Geosciences, University of Edinburgh, Edinburgh, EH9 3FE, UK

<sup>3</sup>Met Office, Exeter, EX1 3PB, UK

## Correspondence

Ashar A. Aslam, School of Earth and Environment, University of Leeds, Leeds, LS2 9JT, UK

Email: eaaaas@leeds.ac.uk

## Funding information

Aslam received funding from NERC through a SENSE CDT studentship (NE/T00039X/1).

Peatman and Birch were funded through the TerraMaris project (NE/R016739/1).

Patterns in extreme precipitation across the Maritime Continent in Southeast Asia are known to be modulated by many processes, from large-scale modes of variability such as the Madden-Julian Oscillation, to finer-scale mechanisms such as the diurnal cycle. Transient mid-level dry air intrusions are an example of a feature not extensively studied over the Maritime Continent, which has the potential to influence rainfall patterns. Here, we show that these dry air intrusions originate from upper-level disturbances along the subtropical jet. Mid-level cyclonic circulation anomalies northwest of Australia from December-February (DJF) intensify westerlies in the southern Maritime Continent, advecting dry air eastward. In contrast, mid-level anticyclonic circulation anomalies northwest of Australia from June-August (JJA) intensify southern Maritime Continent easterlies, advecting dry air westward. The resultant transport direction of associated air parcels is also dependent on the seasonal low-level monsoon circulation. Dry air intrusions are important in influencing low-level wind and rainfall patterns, suppressing rainfall over seas near the southern Maritime Continent in both seasons, as well as over southern Maritime Continent islands in DJF, and the Indian Ocean in JJA. In both seasons, there is enhanced rainfall to the east of the in-

This article has been accepted for publication and undergone full peer review but has not been through the copyediting, typesetting, pagination and proofreading process which may lead to differences between this version and the [Version of Record](#). Please cite this article as doi: [10.1002/qj.4618](https://doi.org/10.1002/qj.4618)

trusion, where there is moist return flow to the extratropics. This study highlights the importance of synoptic-scale extratropical features in influencing meteorological patterns in the tropics.

#### KEYWORDS

Dry air intrusions, Maritime Continent, rainfall, deep convection, tropical-extratropical interactions

## 1 | INTRODUCTION

The Maritime Continent (MC) in Southeast Asia consists of an archipelago of thousands of islands and several shallow seas (Figure 1a). High sea surface temperatures (SSTs) and variable topography make the region conducive to the formation of deep convection all year round. Rainfall over the MC (Figures 1b-c) is twice the global mean (Yamanaka et al., 2018), with mean precipitation rates exceeding  $10 \text{ mm day}^{-1}$  (Ichikawa and Yasunari, 2006). The associated latent heat release influences the global atmospheric circulation and climate through Rossby wave generation and subsequent propagation towards the extratropics (Jin and Hoskins, 1995). The MC has therefore been termed an 'atmospheric boiler box' (Ramage, 1968).

Deep convection over the MC encompasses multiple spatial and temporal scales, and several mechanisms modulate precipitation patterns. These processes include the diurnal cycle of solar heating (e.g. Mori et al., 2004; Qian, 2008; Yokoi et al., 2017), large-scale modes of variability such as the Madden-Julian Oscillation (MJO; e.g. Madden and Julian, 1971, 1972, 1994), the El Niño Southern Oscillation (ENSO; e.g. Haylock and McBride, 2001), the Indian Ocean Dipole (IOD; e.g. Saji et al., 1999; Saji and Yamagata, 2003), and equatorial waves (e.g. Wheeler and Kiladis, 1999; Yang et al., 2003; Ferrett et al., 2020). Scale interactions also exist between processes, adding further variability, and therefore complexity, to our understanding of convective organisation, water vapour profiles and cloud structure over the MC (e.g. Rauniyar and Walsh, 2013; Peatman et al., 2014, 2021). Limitations in our knowledge of these mechanisms lead to errors in model-simulated precipitation patterns over the MC primarily due to issues in resolving finer-scale features, or because of the parameterisation design (e.g. Yang and Slingo, 2001; Neale and Slingo, 2003; Qiani, 2008; Birch et al., 2016; Vincent and Lane, 2016).

Another feature with the potential to influence regional precipitation patterns are dry air intrusions (DAIs), which are descending tongues of low specific, and relative, humidity and high potential vorticity (PV), 100s of kilometres in width, injected from the upper-troposphere/lower-stratosphere (Danielsen, 1968; Appenzeller and Davies, 1992; Browning, 1997). Extratropical wave trains act as a source of DAIs, as shown by back trajectory analysis (e.g. Casey et al., 2009) and neural networks (Silverman et al., 2021). Amplification of disturbances along the upper-level subtropical jet leads to isentropic folding of the tropopause and anticyclonic Rossby wave breaking, forcing descent of upper-level dry air (Numaguti, 1995; Bithell et al., 1999; Funatsu and Waugh, 2008). The resultant direction that dry air is transported depends on factors such as the jet position and the background wind field (Homeyer and Bowman, 2013).

The frequency of DAI events has large spatial variability. Waugh and Polvani (2000), Stohl (2001), Casey et al. (2009) and Raveh-Rubin (2017) produced climatologies of DAI occurrence (the latter two offering global coverage). DAIs are most prevalent over the Pacific and Indian Oceans, occurring more often in the winter season for each hemisphere. However, they contribute to anomalously dry air all year round.

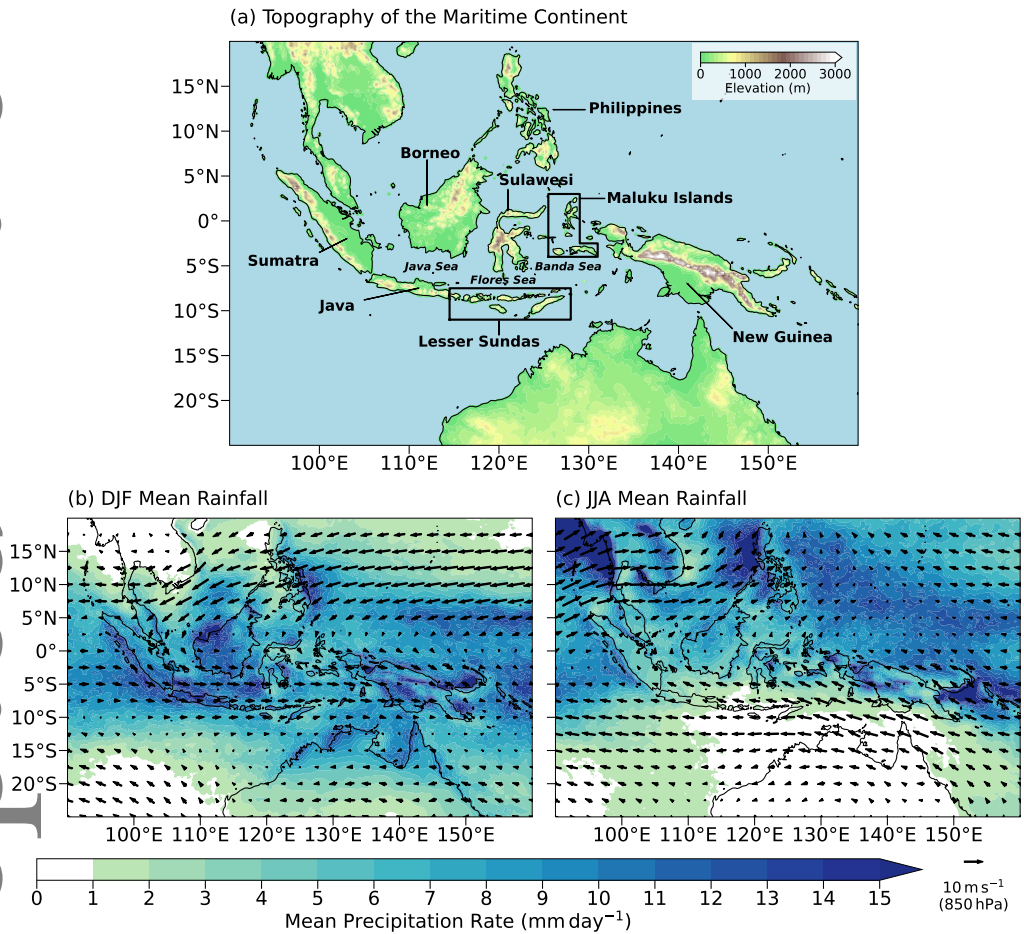


**FIGURE 1** (a) Map showing the topography/elevation of the Maritime Continent, with some of its constituent islands and seas labelled. Panels (b) and (c) show the climatological means of GPM precipitation rates for (b) DJF (December 2000-February 2001, to December 2019-February 2020) and (c) JJA (June-August 2001, to June-August 2020). Black arrows represent 850 hPa wind.

1 Atmospheric soundings show DAIs sit atop sharp stable layers, produced by anomalous longwave cooling of the  
2 top of the underlying moist air (Mapes and Zuidema, 1996; Zhang and Chou, 1999; Johnson et al., 2001). The radiative  
3 and convective profile in the tropics can therefore be perturbed by humidity fluctuations attributed to DAIs coming  
4 from the extratropics (Brown and Zhang, 1997; Ryoo et al., 2008). Such disturbances can affect the moisture field  
5 and the low-latitude circulation, thereby impacting regional meteorology and environmental conditions (e.g. Rodwell,  
6 1997; Knippertz, 2007).

7 Localised, transient breaks in tropical precipitation on daily-to-weekly timescales can be associated with DAIs.  
8 This link has been observed in regions such as the tropical West Pacific during the Tropical-Ocean Global-Atmosphere  
9 Coupled Ocean-Atmosphere Response Experiment (TOGA COARE; e.g. Mapes and Zuidema, 1996; Yoneyama and  
10 Parsons, 1999; Lucas and Zipser, 2000; Lucas et al., 2000; Parsons et al., 2000) and the Indian subcontinent, such  
11 as through the Interaction of Monsoon Precipitation and Convective Organization, Atmosphere, Surface and Sea  
12 (INCOMPASS) project (e.g. Parker et al., 2016; Fletcher et al., 2020; Volonté et al., 2020).

13 Mid-level DAIs cap the moist boundary layer, decreasing boundary layer parcel buoyancy and increasing convec-  
14 tive inhibition. Gradual increases in boundary layer equivalent potential temperature and potential instability lead to  
15 convective available potential energy (CAPE) build-up (Brown and Zhang, 1997; Yang et al., 2009; Parker et al., 2016).  
16 Increases in CAPE allow convection to erode the dry air layer, primarily through convective cloud detrainment. Con-  
17 vective recovery is, however, non-steady, being influenced by both local factors, such as the diurnal cycle, orography,  
18 convective structure and surface feedbacks, and remote factors, including synoptic circulations and dynamics origi-  
19 nating from the extratropics (Mapes and Zuidema, 1996; Brown and Zhang, 1997; Redelsperger et al., 2002; Fletcher  
20 et al., 2018; Volonté et al., 2020).

21 DAIs can also result in low-level convergence, vertical motion and increased convection when encountering warm,  
22 moist air masses on eastward margins and leading edges, through isentropic displacement and reductions in potential  
23 stability ahead of upper-level troughs (e.g. Funatsu and Waugh, 2008; Vaughan et al., 2017). Disturbances along the  
24 jet stream and their resultant DAIs can therefore steer and organise deep convection, through which increases in  
25 rainfall may be observed (Allen et al., 2009; Berry and Reeder, 2016). However, the environment near to the intrusion  
26 must be moist enough to be conducive to the formation of deep convection (de Vries et al., 2016, 2018; Kumar et al.,  
27 2019). As DAIs themselves modify the lower-level wind field, they can therefore enhance the moisture flux enabling  
28 convection downstream (Rodwell, 1997; Knippertz, 2007; Ward et al., 2021).

29 Despite insights gained from previous studies across the tropics, DAIs have not been extensively studied in rela-  
30 tion to MC precipitation. Murata et al. (2006) and Seto et al. (2006) used rawinsonde, radar and surface meteorological  
31 data, and identified DAIs over Sumatra. Murata et al. (2006) noted events where there is convective suppression be-  
32 hind and eastward-propagating squall lines. Seto et al. (2006) found this suppression to be associated with intensification  
33 of westerly winds. More recently, Feng et al. (2021) used the Sumatran GPS (Global Positioning System) array to in-  
34 vestigate summer intraseasonal variability in precipitable water vapour, a property which influences the propagation  
35 of the satellite signal. DAIs over Sumatra were associated with interactions linked to Rossby waves propagating in  
36 the Southern Hemisphere mid-latitudes. However, these studies use a small number of events in their analysis and  
37 do not explicitly analyse impacts on rainfall in the region.

38 Rodwell (1997) highlighted that limits to the accuracy of seasonal forecasts and predictability of rainfall can be  
39 influenced by synoptic-scale/transient events such as DAIs, particularly if a single event provides significant contribu-  
40 tions to the seasonal anomaly. Anomalies associated with DAIs could represent a significant challenge for accurate  
41 seasonal forecasts as the slowly-varying lower boundary conditions, evolving from initial conditions, cannot anticipate  
42 transient events such as DAIs. Further research into processes regulating regional precipitation will benefit society in  
43 the MC as communities experience serious floods and landslides as a result of extreme weather. Better meteorological

1 understanding will improve forecasting potential and ensure socioeconomic security for the 500 million people living  
2 in the MC, alleviating current vulnerability to disaster and loss (Wijayanti et al., 2017; Narulita and Ningrum, 2018).

3 In this study, we aim to identify mechanisms which enable the occurrence of DAIs and their impact on rainfall  
4 over the southern MC, and to establish any seasonal differences. We use 42 years of ERA5 reanalysis data to identify  
5 dry events near the MC through analysis of variance and anomalies in humidity. Section 2 outlines methods used,  
6 including utilised data, the choice of study location, the workflow in identifying dry events and computation of air  
7 parcel trajectories to determine attribution to DAIs. We present results in Section 3, including parcel trajectories,  
8 regulatory mechanisms of mid-level dry events, and impacts on regional rainfall patterns. Section 4 synthesises these  
9 results to see if there are similarities between this work and past studies, or whether processes and impacts related  
10 to dry events are unique for this region. Conclusions are provided in Section 5.

## 11 2 | METHODS

### 12 2.1 | Data

13 ERA5 reanalysis data, the ECMWF (European Centre for Medium-Range Weather Forecasts) Reanalysis v5 of global  
14 climate and weather (Hersbach et al., 2020), is used to investigate DAIs. Instantaneous hourly ERA5 data - at a  
15 horizontal grid spacing of  $0.25^\circ \times 0.25^\circ$ , equivalent to 26 km - from 1979 to 2021 (42 years) was used. Data was used  
16 for 20 levels from 50 hPa to 1000 hPa at 50 hPa vertical resolution, for the domain of  $20^\circ\text{N}$ - $60^\circ\text{S}$ ,  $60^\circ$ - $160^\circ\text{E}$ . The  
17 hourly data was then used to determine daily means for each variable across the domain. Daily mean rainfall data from  
18 the Global Precipitation Measurement (GPM) mission, pre-processed using the Integrated Multi-Satellite Retrievals  
19 for GPM (IMERG) Version 06 algorithm (Huffman et al., 2020), was also used. The IMERG algorithm inter-calibrates  
20 gauge data with precipitation estimates from satellite infrared and microwave sensors. GPM data was available at  
21  $0.1^\circ \times 0.1^\circ$  horizontal grid spacing, for 20 years from December 2000 to November 2020.

22 Daily means were averaged over all years for each variable to produce a climatological mean daily annual cycle,  
23 which was later smoothed using a 30-day mean.

### 24 2.2 | Dry Event Identification

25 The analysis of the variance in daily mean specific humidity at 700 hPa was conducted for each season, in order to  
26 identify regions exhibiting fluctuations in mid-level humidity. A box was selected based on the spatial pattern of  
27 the variance. As shown in Figure 2a, highest variance in mid-level specific humidity is observed either side of the  
28 MC. Prominent locations of high variance include the eastern Indian Ocean southwest of Sumatra and Java, and the  
29 southwestern tropical Pacific Ocean near New Guinea and Australia. A box was selected covering the region of  $9^\circ$ -  
30  $20^\circ\text{S}$ ,  $95^\circ$ - $115^\circ\text{E}$ , near to Sumatra and Java. This box encloses the eastern periphery of the first high variance region  
31 identified, located between  $10^\circ$ - $20^\circ\text{S}$  and  $80^\circ$ - $100^\circ\text{E}$ .

32 The presented method of identifying dry events is illustrated schematically in Figure 2b. Anomalies in 700 hPa  
33 daily mean specific humidity were first calculated relative to the associated days and months within the smoothed  
34 mean annual cycle, averaged over the identifier box. These anomalies were then normalised by dividing by that same  
35 day within the smoothed mean annual cycle. Dry days were defined as days where normalised specific humidity  
36 anomalies are below the 5th percentile, computed for each season from 1979/80 to 2020/21. If a dry day has a  
37 normalised specific humidity anomaly more negative than the 10 days preceding and following it, the dry day repre-  
38 sents the middle, or 'Day 0', of a dry event, which is a local humidity minimum. This method is chosen so that events

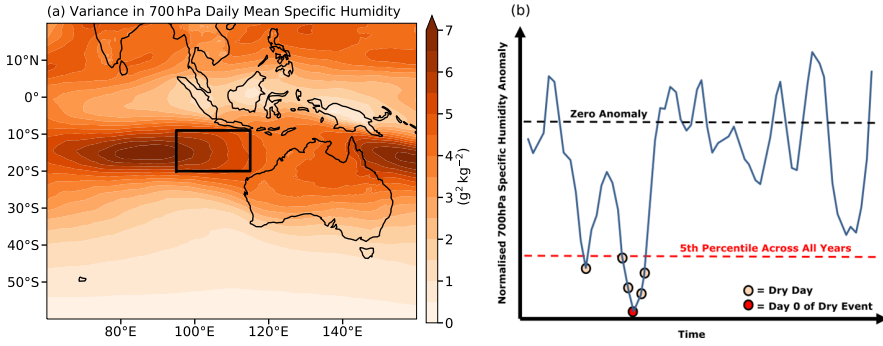


**FIGURE 2** (a): Variance in daily mean specific humidity at 700 hPa for the entire time period of analysis from December 1979 to November 2021. The black box ( $9^{\circ}$ - $20^{\circ}$ S,  $95^{\circ}$ - $115^{\circ}$ E) represents the selected region in this study for identification of mid-level dry events. (b): An illustration of the method described for identifying dry events. In blue is a timeseries of normalised 700 hPa specific humidity anomalies for a particular season and year. The black dashed line represents zero anomaly, and the red dashed line represents the 5th percentile of normalised 700 hPa specific humidity anomalies as calculated across all 42 years for a particular season. Beige dots represent dry days, and red dots represent Day 0 of dry events, where the anomaly is at its most negative relative to neighbouring days.

1 associated with an individual DAI are isolated, ensuring they are not accounted for more than once. Effects of DAIs  
 2 are noted up to 8-15 days after an intrusion (in TOGA COARE; e.g. Yoneyama and Fujitani, 1995; Parsons et al., 2000),  
 3 so defining events with a 10-day window either side of a minimum in normalised specific humidity anomalies can be  
 4 justified.

### 2.3 | Trajectory Analysis

5 Lagrangian trajectory analysis is used to track air parcels associated with dry events. Advection of each parcel  
 6 only requires details of the three-dimensional wind field, used to track the location and physical properties of these  
 7 particular parcels for time periods of interest. Trajectories were calculated by determining a first guess (denoted with  
 8 the symbol) position of a parcel at time  $t + \Delta t$ , given by

$$\mathbf{r}'_{t+\Delta t} = \mathbf{r}_t + \mathbf{v}_t(\mathbf{r}_t) \cdot \Delta t, \quad (1)$$

9 where  $\mathbf{r}$  is the three-dimensional spatial co-ordinate of the air parcel, and  $\mathbf{v}$  is the three-dimensional wind velocity  
 10 field at position  $\mathbf{r}$  (e.g. Wernli and Davies, 1997; Draxler et al., 1998).  $\Delta t$  represents the time step, which is 1 day for  
 11 forward trajectory analysis, and -1 day for back trajectory analysis. An adjusted mean wind is determined from  
 12

$$\tilde{\mathbf{v}} = 0.5[\mathbf{v}_t(\mathbf{r}_t) + \mathbf{v}_{t+\Delta t}(\mathbf{r}'_{t+\Delta t})], \quad (2)$$

13 to give the final position of the air parcel

$$\mathbf{r}_{t+\Delta t} = \mathbf{r}_t + \bar{\mathbf{v}} \cdot \Delta t. \quad (3)$$

Trajectories were computed for each grid point within the identifier box (9°-20°S, 95°-115°E) at Day 0, where both latitude and longitude co-ordinates are integers (12×21 points). As ERA5 data is at 0.25° horizontal resolution, and data is downloaded at 50 hPa vertical resolution, when a guess position is not located on these defined grid points or levels, tri-linear interpolation is applied to determine the values of  $\mathbf{v}$  associated with their position  $\mathbf{r}$ . If  $\mathbf{r}$  exists outside the domain (20°N-60°S, 60°-160°E, for vertical pressure levels between 50-1000 hPa), the trajectory is terminated. We find that using a daily-mean wind input does not fundamentally change the mean trajectory path compared to using an hourly input (not shown).

## 2.4 | Association with Modes of Variability

Dry events were grouped into associations with the phases of ENSO, IOD and MJO to determine associations between dry events and larger-scale controls. Details on the data representing these modes of variability can be found in Table 1. Ratios were calculated from the frequencies of these events by dividing the fraction of events in each phase relative to the total number of events per season, by the fraction of days in each phase relative to the total number of days in each season across the 42 years. This calculation provides a ratio between event frequency and day frequency with respect to each phase. If this ratio equals 1, the phase is as likely to occur during dry events as it is all days. If the ratio is 2, then the phase is twice as likely to occur during dry events.

Statistical significance of links between dry event occurrence and large-scale modes of variability was tested through bootstrapping. For each season, we randomly subset a set of days of equivalent length to the number of events identified per season, where the state of each mode for each day is determined. We perform the calculations as described previously for these sets of days, relative to the distribution of days in the whole season across the phases of each mode. This process is repeated 1000 times to produce a distribution of ratios for the state of each mode for each season. Percentiles for the original ratios relative to the bootstrapped distribution are then calculated. These percentiles allow the determination of the significance of association with modes of variability relative to a selected confidence interval.

## 3 | RESULTS

This section outlines the results obtained from this study. Section 3.1 provides details on the number of identified dry events, outcomes from parcel trajectory analysis for case studies, and for all dry events. Section 3.2 seeks to provide reasoning for such trajectories through understanding mechanisms regulating the occurrence of dry events. Statistical links between dry event occurrence and phases of various modes of variability are provided in Section 3.3. Lastly, Section 3.4 shows the results in analysing changes to rainfall patterns during dry events.

### 3.1 | Dry Event Characteristics and Parcel Trajectories

Employing the chosen method described in Section 2.2, we identify 201 dry events over the 42-year period of analysis. Focusing on DJF and JJA, we find 47 and 56 dry events respectively, equivalent to just over 1 event per season, per



**TABLE 1** The indices used in analysing links between the states of selected modes of variability and the occurrence of dry events. Details on their derivation and the definition of events related to the various modes are also provided. The sources for the indices are noted in the Acknowledgements.

Mode	Index and Derivation	Event Definition
ENSO	Monthly Ocean Niño Index (ONI; NOAA, 2019) - derived from the average temperature anomaly in the surface waters of the central-eastern tropical Pacific.	El Niño events are defined where $ONI \geq 0.5^{\circ}\text{C}$ for 5 successive months, and La Niña events are defined where $ONI \leq -0.5^{\circ}\text{C}$ for 5 successive months.
IOD	Monthly IOD Dipole Mode Index (DMI; Saji and Yamagata, 2003) - derived from the anomalous sea-surface temperature gradient between the the western equatorial and southeastern equatorial Indian Ocean.	Positive IOD events are defined where $DMI \geq 0.4^{\circ}\text{C}$ for 3 successive months. Negative IOD events are defined where $DMI \leq -0.4^{\circ}\text{C}$ for 3 successive months.
MJO	Daily real-time Multivariate MJO series 1 and 2 (RMM1 and RMM2) - the principal components of the two leading empirical orthogonal functions (EOFs), defined by EOF analysis of the combined field of outgoing longwave radiation and wind, which define the phase of the MJO (Wheeler and Hendon, 2004). The amplitude is defined as $\sqrt{RMM1^2 + RMM2^2}$ .	MJO events occur when the amplitude for a specific day exceeds or is equal to 1. Where the MJO amplitude is below 1, we label an event as being under 'Phase 0'.

1 year.

We first analyse where air parcels associated with identified dry events originate from and are advected to, using the parcel trajectory equations provided in Section 2.3. Initial analysis is performed on select events, and Figure 2 shows results for events which had normalised specific humidity anomalies equivalent to the event-average per season. These are the 9th January 2020 (Figure 3a-c) and 26th July 2020 (Figure 3d-f) dry events for DJF and JJA respectively.

Back trajectory analysis shows that air parcels associated with the selected DJF dry event originate largely from the extratropics in the southeast Indian Ocean ( $30^{\circ}$ - $50^{\circ}\text{S}$ ), 6-9 days prior to the peak of the dry event (Figure 3a), descending from 200-500 hPa (Figure 3c). Forward trajectories show that, on average, air parcels remain confined within near-equatorial latitudes from  $5^{\circ}$ - $20^{\circ}\text{S}$  (Figure 3b), descending further to the near-surface for up to 10 days after the peak of the dry event before re-ascending to upper-levels (Figure 3c). Some parcels however rapidly ascend just after Day 0. Most air parcels are advected eastward towards New Guinea and northern Australia in the southeast, with a slightly smaller portion westward towards the Indian Ocean. Some trajectories recurve back towards the Southern Hemisphere extratropics.

For the selected JJA dry event, air parcels largely originate from the extratropics as well, though slightly further north than in DJF, between  $20^{\circ}$ - $40^{\circ}\text{S}$ , in the southeastern Indian Ocean 3-6 days prior to the peak of the dry event (Figure 3d), descending from the upper-levels between 300-500 hPa (Figure 3f). An additional (albeit much smaller) source of air parcels is located over the tropics around New Guinea and the western Pacific, up to 12 days prior to the peak. Forward trajectories show that most air parcels are advected towards the eastern Indian Ocean, within 6 days of the peak (Figure 3e). After this, up to 15 days after the peak of the dry event, many trajectories are directed northeastward towards mainland Southeast Asia and the northern MC. Few trajectories return to the extratropics to the south of Australia. On average, air parcels continue descending in some cases beyond 10 days after the peak of

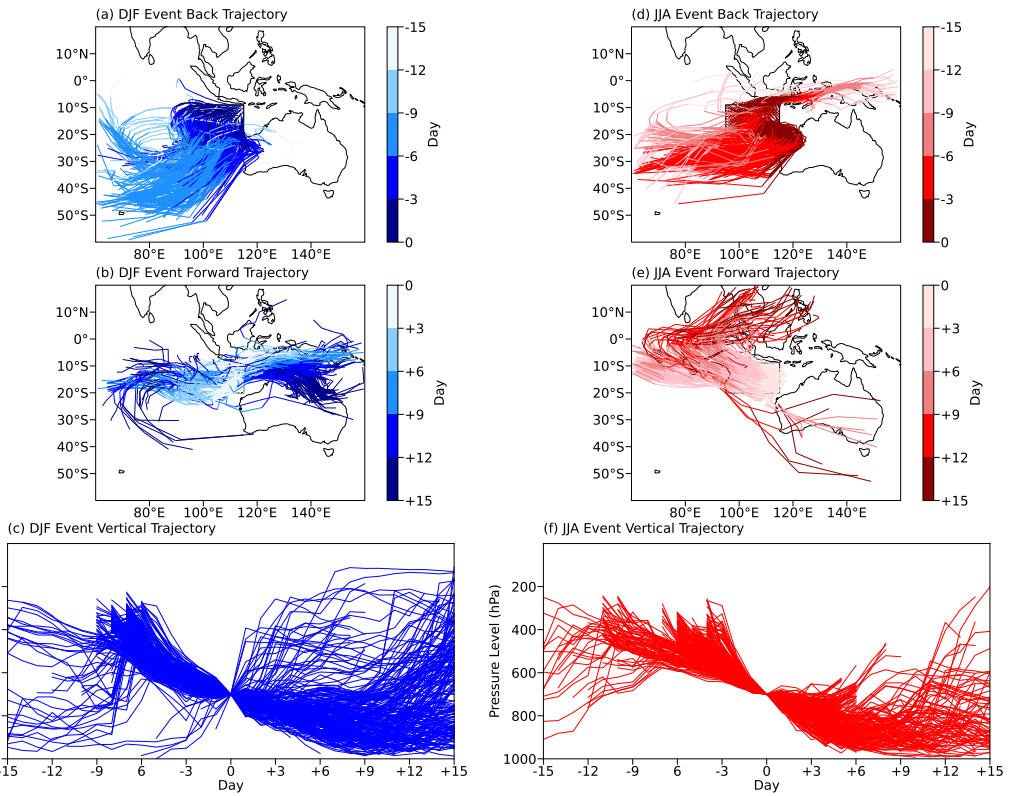


**FIGURE 3** Air parcel trajectories for the (a-c) 9th January 2020 DJF and (d-f) 26th July 2020 JJA dry events. From top to bottom, panels represent back, forward and vertical trajectories, respectively.

the dry event (Figure 3f).

In Figure 4, we show the distribution of air parcels associated with all dry events in DJF and JJA, to corroborate the above analysis based on individual events. Blue and red contours represent the limits of the trajectory to the number of days listed above the figure panels for DJF and JJA respectively. Filled contours represent the difference between these distributions, where blue (red) represents where more DJF (JJA) air parcels are located. The JJA distribution is re-scaled to have the same number of parcel trajectories as DJF, by multiplying the distribution in JJA by the number of events in DJF (47), divided by the number in JJA (56).

10-15 days before the event, JJA parcels are located further to the north of the MC between  $0^{\circ}$ - $15^{\circ}$ S and  $80^{\circ}$ - $100^{\circ}$ E, while DJF parcels are located further south over the Indian Ocean between  $15^{\circ}$ - $35^{\circ}$ S and  $60^{\circ}$ - $130^{\circ}$ E. (Figure 3a). Going forward in time, average trajectories suggest parcels most commonly enter the domain from the upper-troposphere between 200-500 hPa (Figure 4g) and extratropics over the southern Indian Ocean to the west (Figures 4b). This is observed most strongly during DJF 5-10 days before the peak of the dry event, but also in JJA. Just before the peak of the dry event, most DJF parcels are close to the identifier box where trajectories began (Figure 4c). However, the JJA distribution suggests parcels can come from the extratropics during the 5 days before the event peak, with some advected southwestward from the tropics. The extratropical source to the southwest is however common to both DJF and JJA regardless of how far back in time one goes, though JJA has an additional (yet smaller)

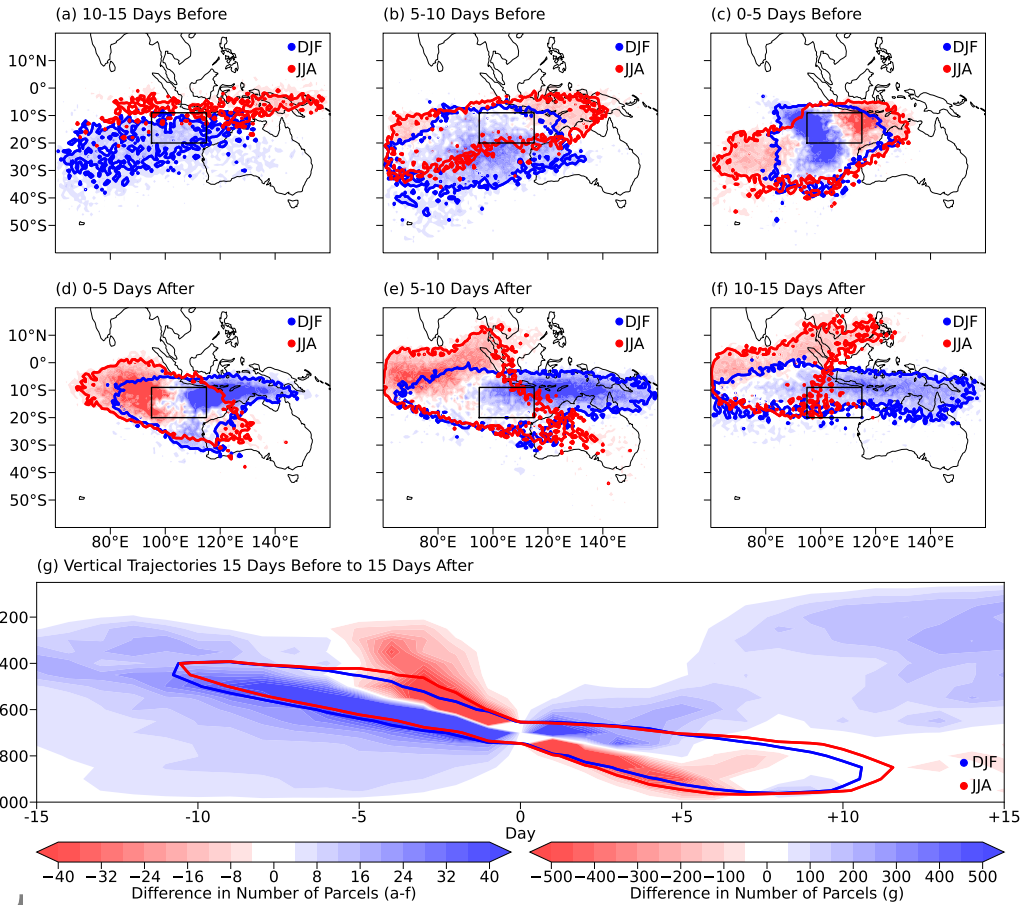


**FIGURE 4** The distribution in dry event-related air parcels as calculated through (a-c) back and (d-f) forward trajectory analysis. Blue and red contours represent the limits of the trajectory to the number of days listed above the figure panels for DJF and JJA respectively. This is indicated by contours where the sum of parcels across the days, labelled above the figure panels, is 10 parcels. Filled contours represent differences between the distribution in each season, where the difference is the JJA distribution subtracted from the DJF distribution, where the JJA distribution is re-scaled to have the same number of parcel trajectories as DJF, done by multiplying the distribution in JJA by the number of events in DJF (47), divided by the number in JJA (56). This re-scaling allows a difference between JJA and DJF to be calculated (otherwise there will be a tendency for differences to shift towards the negative with more parcels present in the domain in JJA than DJF, by virtue of the difference in number of events). Panel (g) shows the distributions for each season as a function of time and vertical pressure level, summed over all longitudes and latitudes. Blue and red contours represent the limits of the vertical trajectory to the day labelled on the x-axis for DJF and JJA respectively. These limits are indicated by contours where the sum of parcels is 1000 parcels.

1 source coming from the tropics east of New Guinea.

2 Up to 5 days after the dry event peak, DJF parcels are mostly advected eastward across the MC towards New  
3 Guinea, with some also advected westward (Figures 4d). Up to 10 days after the event, the eastward propagation  
4 noted in DJF persists (Figure 4e). Compared to DJF, JJA parcels are, on average, advected northwest towards India,  
5 while some are also advected northeastward over Sumatra and Malaysia towards mainland SE Asia (Figures 4d-f).

6 Air parcels associated with the trajectories linked to dry events have characteristic descent from 10 days before  
7 the event peak, to 10 days after (Figure 4g). However, DJF parcels, compared to JJA, originate from the upper-levels  
8 further back in time, taking longer to descend to the mid-levels. After the event, JJA parcels have a stronger descent  
9 signal compared to DJF, which has a broader vertical distribution, linked to an increase in the number of parcels which  
10 end up re-ascending to the upper-levels.

## 11 3.2 | Regulatory Mechanisms

12 Here, we provide insight into mechanisms regulating dry event occurrence for events identified in DJF and JJA. Figures  
13 5 and 6 show lead-lag composites of specific humidity anomalies for DJF and JJA events.

14 During DJF, up to 7 days before the peak of the dry event, a moist anomaly develops over northern Australia  
15 (Figure 5a). Mid-level westerly anomalies form over the southern MC, with a mid-level cyclonic circulation anomaly  
16 developing northwest of Australia. Between Days -4 and -2, a dry anomaly south of the MC evolves, driven by  
17 southerly advection from the extratropics (Figure 5b). At upper-levels, this advection is linked to disturbances along  
18 the subtropical jet, where a cyclonic circulation anomaly develops southwest of Australia, bounded by anticyclonic  
19 circulation anomalies either side. Mid-level circulation anomalies almost parallel those at the upper-levels, extending  
20 further northward towards the MC. Westerlies over the southern MC are enhanced, and the intensified return flow  
21 to the extratropics east of the mid-level cyclonic anomaly increases the moist anomaly over Australia.

22 Around Day 0, while the dry anomaly intensifies, upper-level disturbances in the extratropics dissipate (Figure 5c).  
23 However, the anticyclonic circulation anomaly over Australia persists, resulting in a preserved moist anomaly there.  
24 The mid-level cyclonic circulation anomaly near the MC develops a NW-SE tilt, centred just off of northwestern  
25 Australia, and the previously enhanced westerlies begin to weaken. Between Days +2 to +4, the dry anomaly begins  
26 to dissipate and spreads out longitudinally, with the moist anomaly over Australia also reduced (Figure 5d). Anomalous  
27 mid-level westerlies in the southern MC are weaker than prior to the dry event peak, linked to the weakened mid-level  
28 cyclonic anomaly.

29 For JJA, between Days -7 and -5, a dry anomaly forms to the east over northern Australia and seas adjacent  
30 to the MC islands (Figure 6a). This anomaly stems from upper-level disturbances further east over eastern Australia,  
31 with southeasterly advection towards the MC. However, composite mid-level wind anomalies here are weak. The pre-  
32 existing dry air migrates westward over Java, the Lesser Sundas, South Sulawesi, the Maluku Islands, and neighbouring  
33 seas (Java and Flores; Figure 1a) between Days -4 and -2 (Figure 6b). A new upper-level disturbance develops to the  
34 southwest of the selected box over the southeastern Indian Ocean, leading to southerly-to-southeasterly advection  
35 at the upper-levels. This advection is linked to an anticyclonic circulation anomaly, intensifying easterlies at mid-levels  
36 to the west of the MC, as well as dry air advection into the tropics.

37 Around Day 0, strong upper-level anticyclonic and cyclonic circulation anomalies are observed to the west and  
38 over Australia respectively (Figure 6c). A mid-level anticyclonic circulation anomaly extends into the tropics, increasing  
39 the intensity of the dry anomaly. The dry anomaly is centred to the south of the MC, though is spread over Java and  
40 adjacent seas, due to pre-existing dry air advected from the east. The mid-level circulation anomaly is tilted NW-SE,  
41 with moist anomalies either side of the dry anomaly of similar tilt. The days following Day 0 are associated with

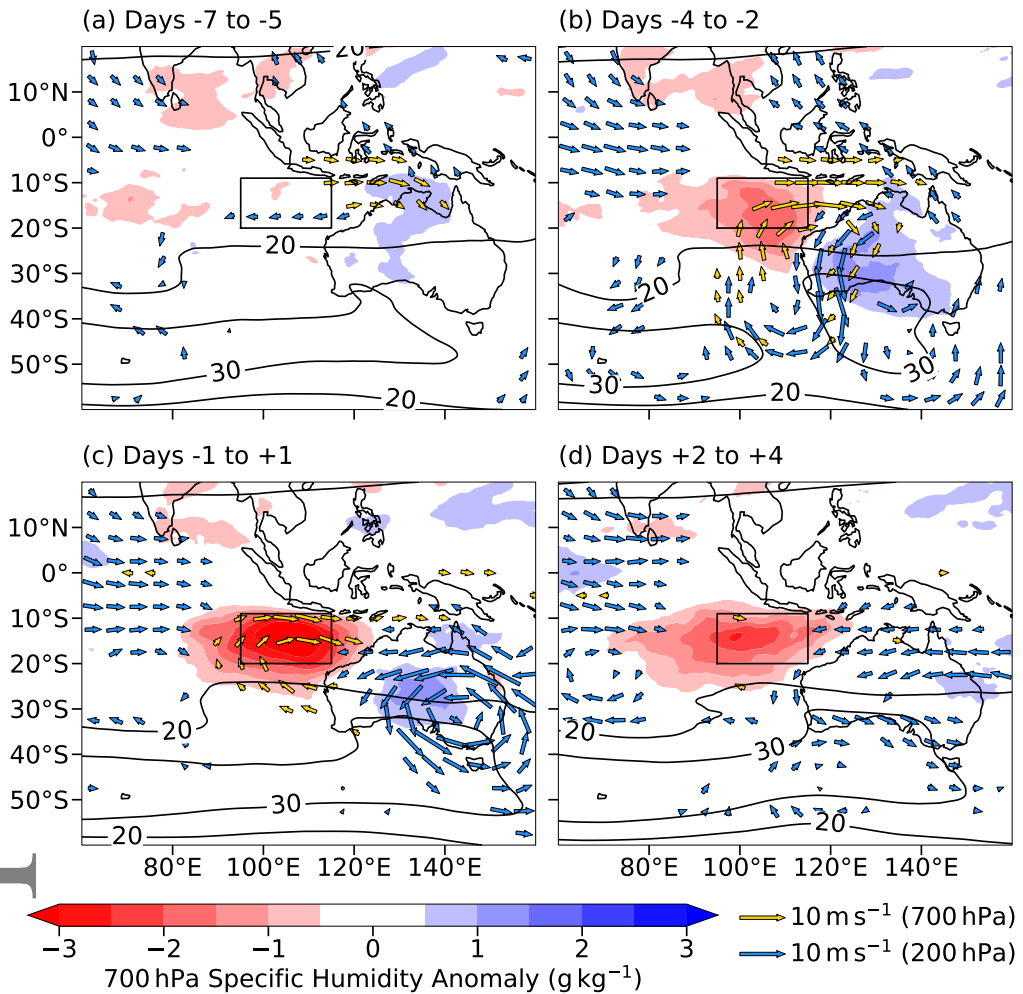


**FIGURE 5** Lead-lag composites for 700 hPa specific humidity anomalies for the 47 dry events identified in DJF from 1979/80 to 2020/21 for (a) Days -7 to -5, (b) Days -4 to -2, (c) Days -1 to +1 and (d) Days +2 to +4. Yellow and blue arrows represent composite 700 hPa and 200 hPa anomalous wind respectively, calculated as the average of wind anomalies for each event relative to the DJF mean annual cycle. Anomalous wind at each level less than  $2 \text{ m s}^{-1}$  is not shown. Black contours represent 200 hPa wind speed at  $20 \text{ m s}^{-1}$  and  $30 \text{ m s}^{-1}$ , indicating the position of the F subtropical upper-level jet. The black box represents the domain used for identifying dry events as in Figure 2.

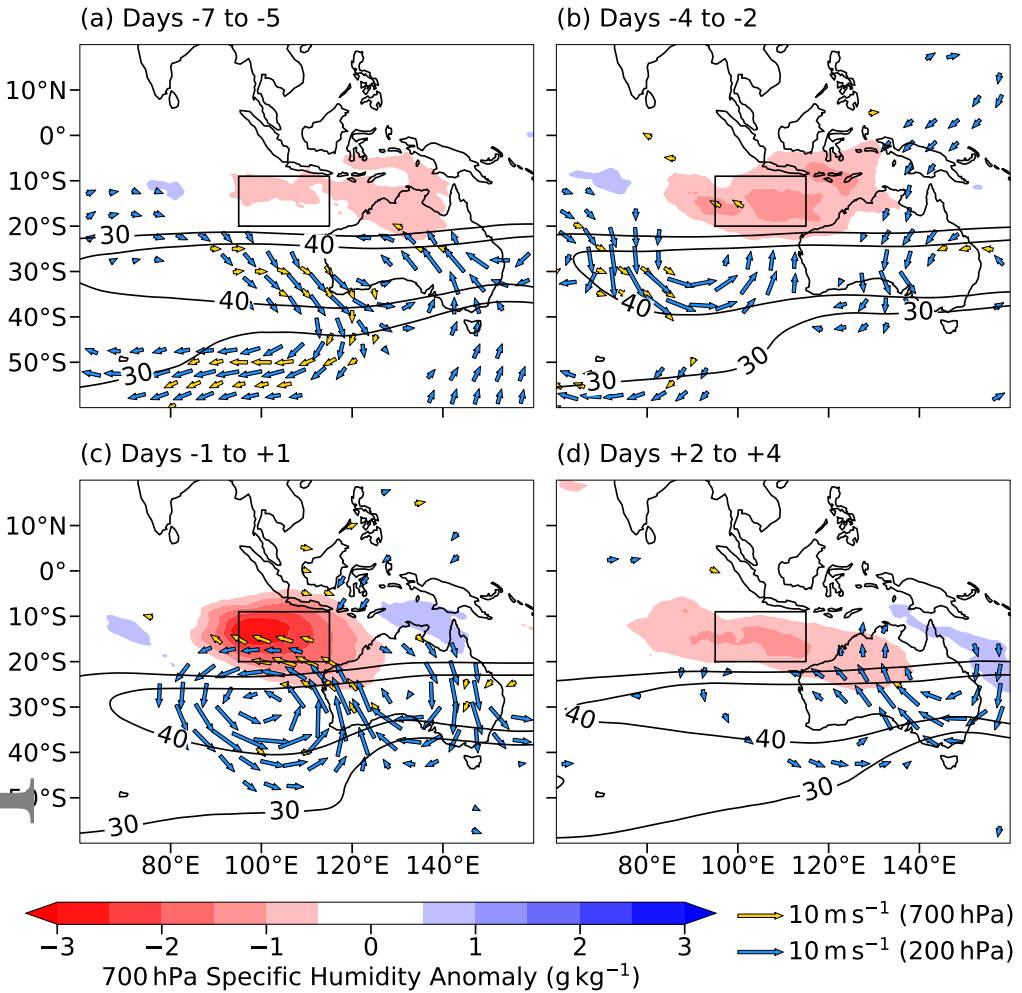


**FIGURE 6** As in Figure 5, but for the 56 dry events identified in JJA.

dissipation of upper-level anomalies near the tropics, with propagation of anomalies further to the east (Figure 6d). These anomalies lead to a new stream of anomalous dry air passing over Australia. Dry air originally near the MC spreads out longitudinally, and the moist anomaly has propagated further east.

In both DJF and JJA, circulation anomalies at both upper-levels and mid-levels are observed. Figure 7 shows time-longitude cross sections of geopotential height for Days -7 to 0, for both the upper-level extratropics and mid-level near-tropics (identifier box region) for both seasons. The choice of these boxes at these levels are in line with the geographical positions of upper- and mid-level circulation anomalies noted in Figures 5-6. In DJF, cyclonic anomalies prior to the peak of the dry event are associated with an upper-level trough in the extratropics, which is strongest at Day -3 (Figure 7a). Descent accompanies the southerly advection of dry air to the west of the trough. Anomalies at the mid-levels can also be linked to a persistent mid-level ridge and trough (Figure 7b). While the ridge does not significantly intensify over time, the trough deepens around Day -3. On the other hand, the prevalent extratropical anticyclonic anomaly in JJA is attributed to an upper-level ridge (Figure 7c). In contrast to DJF, the mid-level trough is not observed to be more intense than the ridge to the west (Figure 7d). Anomalies of descent accompany the southeasterly advection to the east of the ridge.

Results here show that upper-level disturbances within the subtropical jet, developing around 5 days prior to the dry event peak, are a key precursor to dry event occurrence in both seasons. These disturbances drive descent of dry air towards the tropics. In addition, enhancement in mid-level cyclonic circulation centred over northwestern Australia strengthens mid-level southerlies in DJF, enabling advection of dry air towards the MC. This circulation also produces anomalous southern MC westerlies which advect dry air eastward. On the other hand in JJA, an enhancement in mid-level anticyclonic circulation just to the west of Australia strengthens mid-level southerlies, though directing dry air to the same region as in DJF. This circulation too enhances easterlies south of the MC which advects dry air westward towards the Indian Ocean. For both seasons, these dry events can therefore be associated with DAIs. Gradual weakening of enhanced wind circulations in DJF and JJA lead to eventual dissipation of the dry anomalies. In both seasons, moist anomalies are observed to the east of the intrusion, tilted in a direction paralleling the trajectory of dry air.

### 3.3 | Association with Modes of Variability

The previous section established anomalous circulations unique to DJF and JJA which acted as key regulatory mechanisms to the onset of a dry event. These circulations could be due to the state of the large-scale environment as modulated by modes of variability.

To investigate this possible link, the dry events in DJF and JJA were grouped into their associations with the state of ENSO, IOD and MJO, as shown in Table 2 under columns labelled 'Frequency'. These values were converted to ratios as described in Section 2.4, with results shown in columns labelled 'Ratio'.

No statistically significant associations between dry events and the state of ENSO or IOD in either season is found. The MJO on the other hand shows statistically significant links with dry events in each season. In DJF, the MJO is significantly more (nearly twice as) likely to be in Phase 8-1, and significantly (nearly four times) less likely to be in Phases 2-3 when there is a dry event. In JJA, the MJO is significantly more likely to be in Phases 2-3 and Phases 4-5, and significantly (two times) less likely to be in Phases 8-1 when a dry event occurs. Following the associations between geographical location and MJO phase as in Wheeler and Hendon (2004), the MJO active envelope is more likely to be away from (near to) the MC when a dry event occurs in DJF (JJA), and vice versa. Therefore, there appears to be seasonal differences in associations between phase of the MJO and dry event occurrence.

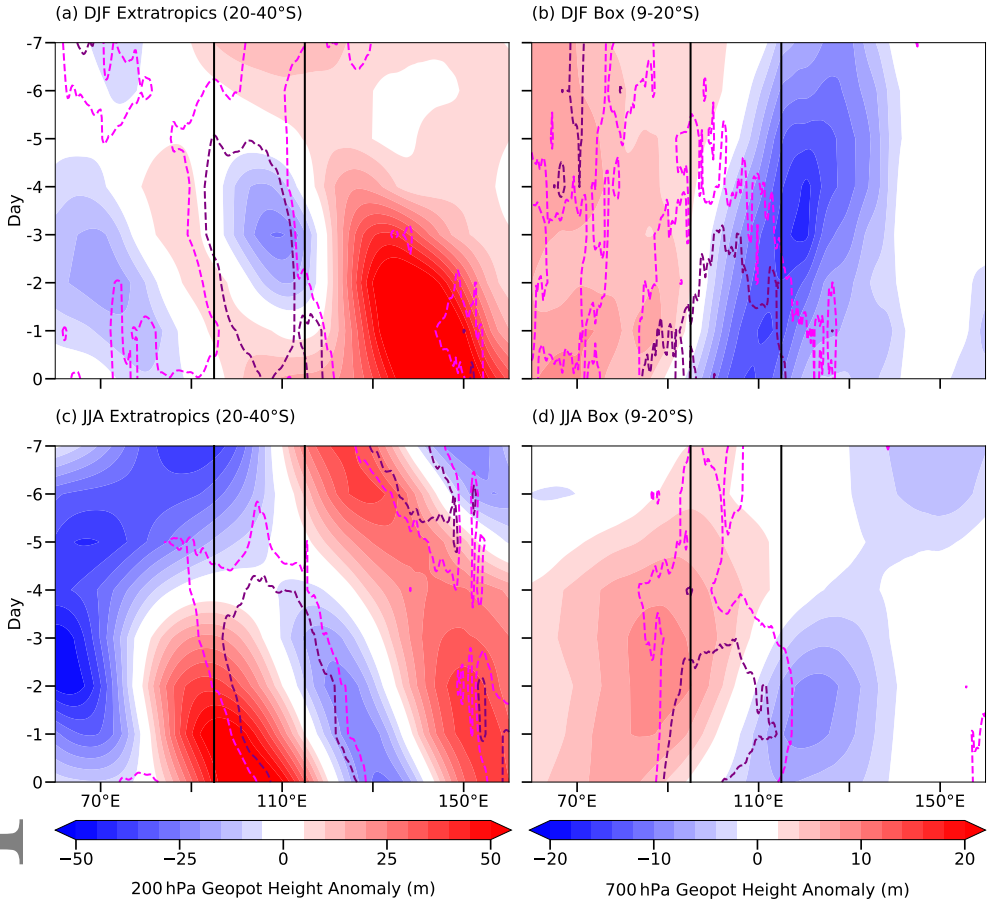


**FIGURE 7** (a-b) Hovmöller plots of 200 hPa and 700 hPa geopotential height anomalies from Day -7 to 0 for the 47 dry events identified in DJF from 1979/80 to 2020/21. Anomalies at 200 hPa are averaged over 20°-40°S, and anomalies at 700 hPa are averaged over 9°-20°S. (c-d) are the same as in (a-b), except for the 56 dry events identified in JJA. Black lines represent the longitudinal limits of the identifier box as in Figure 2. For panels (a) and (c), pink and purple dashed contours represent 0.005 Pa s<sup>-1</sup> and 0.010 Pa s<sup>-1</sup> vertical velocity anomalies respectively, indicating regions of descent. Pink and purple contours in panels (b) and (d) represent 0.010 Pa s<sup>-1</sup> and 0.020 Pa s<sup>-1</sup> vertical velocity anomalies respectively.



**TABLE 2** Dry event frequency ('Frequency') for both DJF and JJA across the states of each mode of variability analysed. Provided are ratios indicating event frequencies compared to the number of days within each season associated with each state of each mode ('Ratio') as described in Section 2.4. Percentiles of these ratios are obtained by comparison to the distribution of 1000 bootstrapped samples, also described in Section 2.4. Where these percentiles are below the 5th percentile or above the 95th percentile, ratios are highlighted in bold and are italicised. MJO phases are associated with geographical locations as follows: Phases 2 and 3 (Indian Ocean), Phases 4 and 5 (Maritime Continent), Phases 6 and 7 (West Pacific), Phases 8 and 1 (Western Hemisphere and Africa), as per Wheeler and Hendon (2004). Phase 0 represents times when the MJO amplitude is below 1 and therefore weak.

Mode	State	DJF (Frequency)	DJF (Ratio)	JJA (Frequency)	JJA (Ratio)
ENSO	El Niño	16	1.04	12	1.08
	Neutral	15	0.94	31	0.94
	La Niña	16	1.02	13	1.08
IOD	Positive	2	1.79	10	1.25
	Neutral	45	1.01	43	0.98
	Negative	0	0.00	3	0.75
MJO	Phase 0	14	0.87	24	0.99
	P2 and P3	2	<b>0.27</b>	12	<b>1.41</b>
	P4 and P5	7	0.90	8	<b>1.25</b>
	P6 and P7	13	1.29	7	1.04
	P8 and P1	11	<b>1.98</b>	5	<b>0.50</b>

#### 3.4 | Impact on rainfall

In this section, we analyse the impact of decreased mid-level humidity on regional rainfall patterns. We use the dry events that take place in the available GPM data record from 2000/01 to 2019/20 as GPM does not go as far back as ERA5. This subset provides 25 and 27 dry events for DJF and JJA, respectively. Precipitation anomalies associated with each event are composited by lag time, and then normalised with respect to the mean rainfall rate at that grid point per season (Figure 1b-c).

During DJF dry events, negative rainfall anomalies develop over NW of Australia, up to 6-10 days before the peak of the dry event (Figure 8a). The rainfall anomalies become larger and more widespread, aligning with the negative specific humidity anomalies between Days -5 to -2 (Figure 8b). Positive anomalies in normalised precipitation rate are observed to the east over and offshore of the NW Australian coastline. Around Day 0, positive rainfall anomalies dissipate, but continued northward propagation of dry air coincides with decreases in rainfall with strongest reductions at the core of the dry anomaly, south of Java (Figure 8c). Anomalies south of the MC dissipate and disperse after the dry event peak. These are now more prevalent further west towards the Indian Ocean (Figure 8d). Slight negative rainfall anomalies are observed over the Lesser Sundas and the neighbouring Flores and Banda Seas to the northeast (Figure 1a). Between Days +6 and +10, most of the negative rainfall and humidity anomalies have dissipated, though more localised dry air and reduced rainfall signatures persist (Figure 8e).

For JJA dry events, there are pre-existing anomalies of reduced rainfall across the region up to prior to the dry event peak (Figure 8f-g). Rainfall reductions are noted over Java, the Lesser Sundas, south Sulawesi, and the Java and Flores Seas (Figure 1a). Only 2-5 days prior to the dry event peak are anomalies originating from the south observed,

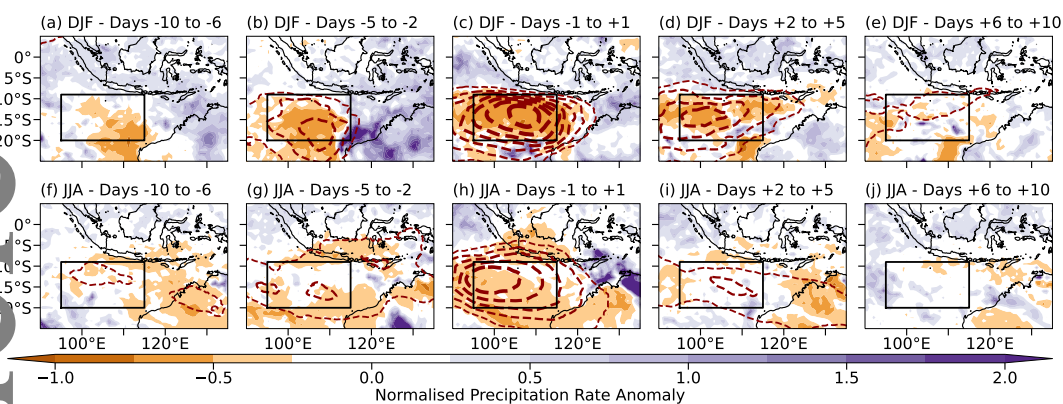


**FIGURE 8** Normalised precipitation rate anomalies with respect to the mean rainfall per grid point for dry events in (a-e) DJF and (f-j) JJA within the available GPM record from 2000/01 to 2019/20 (25 for DJF and 27 for JJA), for Days -10 to +10. Anomalies have been binned into sets of days, with smaller bins closer to Day 0, which each set of data is averaged over. Maroon dashed contours represent negative specific humidity anomalies averaged over these events, where increases in contour thickness reflect decreases (becoming more negative) in the mean specific humidity anomaly by  $0.5 \text{ g kg}^{-1}$ , starting at  $-0.5 \text{ g kg}^{-1}$ . The black box represents the domain used for identifying dry events as in Figure 2.

1 along with negative specific humidity anomalies, just to the northwest of Australia. Increases in rainfall are noted  
 2 the east over Australia. Widespread reductions in rainfall, coinciding with the humidity anomalies, are observed  
 3 around Day 0 (Figure 8h). The pre-existing anomaly from the east leads to reductions over the southern MC. The  
 4 rainfall anomaly from the south shifts northwest towards the Indian Ocean with the reductions in humidity. Positive  
 5 rainfall anomalies develop to the east of the dry anomaly over the Lesser Sundas and northern Australia, with a NW-  
 6 SE tilt. Both negative and positive rainfall anomalies dissipate over the region up to 5 days after the dry event peak  
 7 (Figure 8i). Some anomalies shift westward and southeast towards Australia where there are further reductions in  
 8 rainfall, matching the trajectory of the humidity anomalies. After Day +6, observed anomalies dissipate (Figure 8j).

## 9 DISCUSSION

10 Using the results obtained in Sections 3.1-3.5, we present the mechanisms controlling dry event occurrence and their  
 11 impacts on rainfall in the southern MC schematically in Figures 9a and 9b for DJF and JJA respectively.

12 Analysis of parcel trajectories and precursor anomalies showed that air parcels associated with dry events can be  
 13 attributed to DAIs, originating from upper-level disturbances along the subtropical jet. These processes are likely to be  
 14 related to Rossby wave breaking, as indicated by similar upper-level wind anomaly patterns shown in past studies (e.g.  
 15 Numaguti, 1995). Parallels can also be drawn in terms of dry air sourcing and pathways leading up to a dry event as  
 16 seen in Feng et al. (2021). This work extends Feng et al. (2021)'s observations across a longer time period of analysis  
 17 for more events.

18 Negative humidity anomalies observed coming from the east in JJA up to 7 days prior to the peak of the dry event  
 19 may be attributed to the greater frequency of austral wintertime DAIs (e.g. Casey et al., 2009). Figure 2a highlighted  
 20 a high variance region in mid-level specific humidity between New Guinea and Australia. This region may be where  
 21 the pre-existing dry air originates from, which reaches the MC prior to the analysed intrusions originating from the

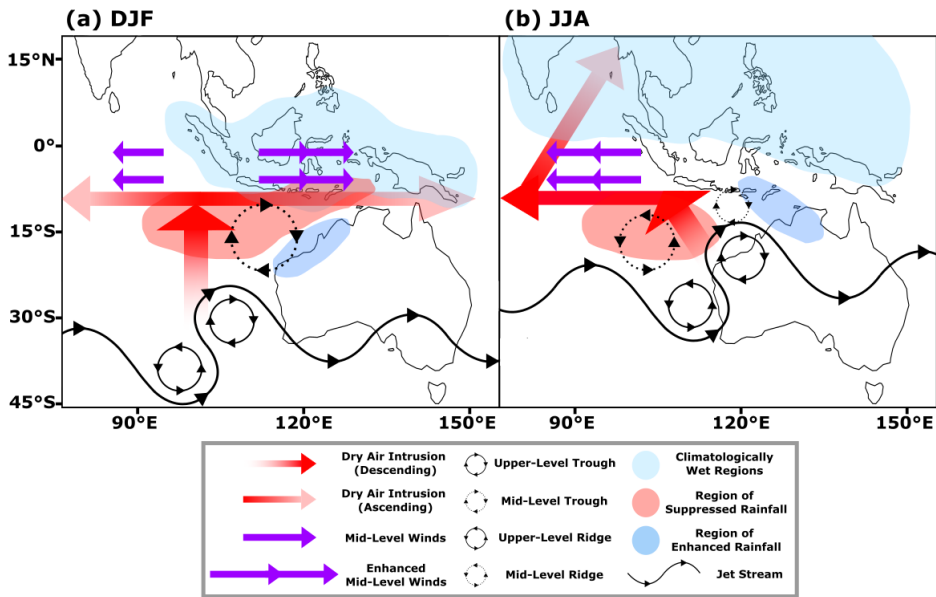


**FIGURE 9** Schematic showing the mechanisms regulating the occurrence of dry events, due to extratropical mid-level DAIs, to the south of the Maritime Continent, and their impacts on Maritime Continent rainfall, for (a) DJF and (b) JJA. Arrow size is not representative of intrusion characteristics - they merely represent direction and vertical motion.

south over the Indian Ocean in JJA.

There are visible differences, however, in terms of the mechanisms regulating the occurrence of dry events in each season. Firstly, air parcels associated with DAIs take less time to arrive into the tropics in JJA compared to DJF, and those found in the domain up to 15 days prior to the dry event peak are located within more equatorial latitudes in JJA than in DJF. This observation is likely to be a product of the northward migration of the subtropical jet and Intertropical Convergence Zone (ITCZ) during the austral winter (as depicted by the shift of the curved black line and light blue region in Figure 9b compared to Figure 9a), as well as strengthening of the jet stream, leading to faster advection of air parcels. However, not all points within the box are dry even when a dry event occurs. Therefore, trajectories starting in the tropics tend to be those not associated with the dry event itself.

Secondly, shifting of the jet northward in JJA is likely to be altering the direction of dry air trajectories into the MC from southerly to southeasterly, with changes to geopotential height anomalies noted. Past studies have found links between jet characteristics and resultant trajectories of DAIs (e.g. Homeyer and Bowman, 2013). However, the observed trough in DJF and ridge in JJA (dotted circles in Figure 9) may be a result of the events which have been composited. The eventual NW-SE tilt attributed to the mid-level trough anomalies in the region of the dry anomaly around Day 0 is expected due to refraction of mid-latitude wave trains towards the tropics (e.g. van der Wiel et al., 2015).

Thirdly, the most pronounced differences between DJF and JJA are in forward trajectories associated with dry events themselves. DJF air parcels have greater re-ascents after the dry event peak (shown as fading red arrows in Figure 9a), compared to that in JJA. In addition, JJA air parcels are advected towards the Indian Ocean, with some further northeast from this position up to mainland Southeast Asia, compared to DJF where there is dominantly eastward

1 advection towards New Guinea, and some advection westward towards the Indian Ocean. The first association is that  
2 the lower-level (850 hPa) climatological wind field, provided in Figure 1b, characteristic of the monsoon circulation in  
3 each season suggest mean westerly motion in the lower-levels in DJF across the southern-central MC, with easterlies  
4 slightly further south, while still within the box latitudes (up to 20°S). The lower-level monsoon circulation explains  
5 the largely eastward propagation of air parcels in DJF after continued descent below 700 hPa. Figure 1c, on the other  
6 hand, shows the opposing monsoon circulation for JJA, where there are strong low-level mean easterlies across the  
7 southern MC, which would explain the largely westward advection of parcels. To the northwest of the MC into the  
8 Indian Ocean near to the Bay of Bengal and mainland Southeast Asia, the low-level monsoon circulation reverses  
9 from northeasterly (as in DJF) to southwesterly, providing reasoning for eventual advection of air parcels towards the  
10 mainland. Parcels, therefore, which continue descent after the peak of the dry event will likely be entrained in the  
11 mean monsoon low-level circulation, influencing their eventual trajectory.

12 Impacts on rainfall generally follow the trajectories presented in Figures 3-4. In both seasons, dry air coming from  
13 the extratropics suppresses rainfall over the sea in the identifier box (red polygons in Figure 9), in agreement with  
14 results from campaigns such as TOGA COARE over the tropical west Pacific (e.g. Parsons et al., 2000). In DJF, dry air  
15 propagates eastward, resulting in a suppressed rainfall signal over the Lesser Sundas of Indonesia, and neighbouring  
16 seas after the dry event. In JJA, rainfall reductions over the islands of the MC are linked to the pre-existing dry air  
17 originating from the east. As JJA trajectories are largely (north)westward, no further reductions over the MC can be  
18 attributed to the studied dry events, though rainfall suppression is apparent going into the eastern Indian Ocean.

19 An increase in rainfall to the east of the dry anomalies, which have a tilt paralleling that of the dry air trajectory  
20 itself, was also observed (blue polygons in Figure 9). When analysing key mechanisms regulating dry events, there was  
21 flow to the extratropics at both mid-levels and upper-levels to the east of troughs, resulting in increases in mid-level  
22 specific humidity. Such moist anomalies are found in similar positions to observed positive rainfall anomalies over  
23 northwestern and northern Australia, as well as the Lesser Sundas, implying that roughly around Day 0, it is possible  
24 to get increases in rainfall just to the east. Berry and Reeder (2016) observed similar positive rainfall anomalies, where  
25 Australian summertime monsoon bursts took place to the east of an upper-level trough. Allen et al. (2009) note  
26 similar increases in tropical convection in this region, and were able to attribute it more directly to the leading edge of  
27 descending dry air mass from the extratropics. Several authors have associated amplification of upper-level troughs  
28 with enhanced convection at the edges and to the east of descending dry air masses elsewhere, thereby steering  
29 convection (e.g. Tompkins, 2001; Pohl et al., 2009; de Vries et al., 2016). DAIs and the associated disturbances  
30 themselves are driving the flow of moist air necessary to form convection, observed in past studies such as Knippertz  
31 (2007) and Ward et al. (2021) over Africa.

32 Our investigation into associations between dry events and large-scale modes of variability (Table 2) found no  
33 significant link between dry event occurrence and both the phases of ENSO and the IOD. Berry and Reeder (2016), for  
34 example, also found no significant link between upper-level troughs, which regulate Australian summertime monsoon  
35 bursts, near to the study region, and ENSO. Pohl et al. (2009) found the opposite results for southern Africa, suggestive  
36 of global variability in associations between upper-level disturbances and the large-scale modes of variability.

37 In contrast with ENSO and IOD, significant links with the MJO have been noted. For DJF, it was observed that  
38 the MJO active phase is significantly more likely to be in Phases 8 and 1 and less likely to be in Phases 2 and 3 when  
39 a dry event occurs. For JJA, when a dry event occurs, the active phase is significantly more likely to be in Phases 2 to  
40 5, and less likely during Phases 8 and 1. In more condensed terms, when a dry event occurs, the MJO active phase  
41 is significantly more likely to be in the vicinity of the MC during JJA, and less likely during DJF. The opposite is noted  
42 when the MJO active phase is away from the region. Therefore, we find similar results to Berry and Reeder (2016) for  
43 DJF (JJA was not examined in their work).

We hypothesise that the link between MJO phase and dry event occurrence is due to circulation anomalies which are driven by the large-scale tropical environment, most dominantly regulated by the MJO on intraseasonal timescales (Madden and Julian, 1971, 1972, 1994), which may be a product of equatorial wave theory associated with MJO dynamics (e.g. Hendon and Salby, 1994; Maloney and Hartmann, 1998; Matthews, 2000). During the active phase, a tongue of low pressure strengthens to the east, associated with a Kelvin wave, with pressure troughs to the northeast and southwest, associated with Rossby waves (Matsuno, 1966; Gill, 1980). The opposite is observed for the suppressed phase of the MJO. The potential for DAI trajectories to be modified by Rossby waves has been past researched over the Indian Ocean in the Dynamics of the MJO (DYNAMO) field campaign (Kerns and Chen, 2014; Chen et al., 2016). Their observations included a strong MJO event and DAIs over the Indian Ocean. A noted interaction linked DAIs to westward-propagating synoptic Rossby gyres in the active envelope. These gyres induced low-level wind circulations drawing the dry air eastward into the equatorial region west of the envelope, contributing to a 1-2 day break in the rainfall during the MJO active phase, favouring a transition to the suppressed phase. This interaction has been validated in various simulations (Wang et al., 2015; Kuznetsova et al., 2019).

Mid-level westerly anomalies persist over the southern MC in DJF (double purple arrows in Figure 9a), linked to the enhanced negative geopotential height anomaly and cyclonic circulation over northwestern Australia. With the strengthened mid-level trough in DJF enhancing both descent of dry air from upper-levels, and equatorward and eastward advection, a similar interaction to that in Kerns and Chen (2014) may be taking place. When the active phase of the MJO is away from the MC, westward-propagating cyclonic circulations, originating from the active envelope, may enhance westerly flow near to the region of study. In the opposite phases, with reversals of anomalous vortices associated with the MJO, there may be easterly intensification, which is the reason for such air parcels propagating westward (single purple arrows in Figure 9a). In JJA, opposite anomalies are noted (Figure 9b), though mid-level easterlies are not as persistent as the westerlies observed in DJF, likely linked to the anomalous geopotential signature being weaker. With dry events more likely when the active phase of the MJO is to the west or over the MC, mid-level ridges (or anticyclonic circulations) are to have greater prevalence near to the region linked with the suppressed phase of the MJO being further to the east. There may be easterly intensification towards the Indian Ocean due to the anticyclonic circulation characteristic of these ridges. Therefore, MJO phase may exert a control on both mid-level circulation and geopotential characteristics noted in each season, potentially interacting with DAIs. Deeper exploration of such associations, however, are beyond the scope of this study and would require further research.

## 5 | CONCLUSIONS

We have investigated the occurrence of dry events south of the Maritime Continent and underlying mechanisms in observations for DJF and JJA. Air parcels associated with dry events in both seasons originate from the extratropics in the southern Indian Ocean as shown by back trajectory analysis, 5-10 days prior to the peak of the dry event. These air parcels are associated with synoptic mid-level dry air intrusions regulated by amplification of upper-level disturbances along the subtropical jet up to 5 days before the dry event peak. Descent of dry air takes place to the west of the upper-level trough and east of the ridge. DJF intrusions are dominated by southerly mid-level advection and a mid-level cyclonic circulation anomaly (trough) northwest of Australia, whereas JJA intrusions have slight southeasterly flow of dry air from the extratropics due to a mid-level anticyclonic circulation anomaly (ridge) northwest of Australia. The circulation anomaly in DJF enhances westerlies in the southern Maritime Continent, allowing advection further east. In contrast, the anomaly in JJA enhances easterlies to the west, enabling westward advection. There are interactions between the low-level monsoon circulation in JJA, where northeasterly flow in DJF near mainland Southeast Asia and

the Bay of Bengal reverses to southwesterly, directing air parcels further northward. Opposing tropical-extratropical flow to the east of intrusions in both seasons transports moisture over Australia and the Lesser Sundas. While, in both seasons, dry air intrusions descend from around 10 days before the peak of the event to 10 days after, there is eventual re-ascend of air parcels in DJF, with more prolonged low-level flow in JJA. Transport mechanisms, influenced by circulation and geopotential anomalies, attributable to dry air intrusion occurrence may be linked to the MJO.

Dry air originating from the extratropics suppresses rainfall, supporting work from other studies analysing convective suppression in the tropics linked to dry air intrusions. Rainfall suppression signatures largely follow intrusion trajectories, where in DJF, reduced rainfall may be found in the southern Maritime Continent over the Lesser Sundas and neighbouring seas, following the eastward propagation. JJA, on the other hand, has limited rainfall reductions over the southern Maritime Continent linked to analysed intrusions. Instead, dry air intrusions originating from further east, leads to reductions over Java, Sumatra, southern Borneo and neighbouring seas. Anomalies linked to the intrusion propagate to the Indian Ocean. In both cases, reduced rainfall can be seen developing around 5 days prior to up to 5 days after the dry event peak. In addition, signatures of positive rainfall anomalies are found to the east of the dry anomalies, indicative of enhanced convection linked to convergence of moist air coming from the tropics to the extratropics encountering the eastward propagation of upper-level disturbances and the negative humidity anomalies. These have been observed elsewhere in the tropics.

This work has extended past work, through usage of 42 years of data compared to select days to weeks in other studies, which were limited by the constraints of observations. However, our approach requires further validation from case study analysis of events linked to dry air intrusions. Such validation is necessary particularly because of the limitations of sample size in terms of number of dry events per season, identified using the employed method. More events are required to provide confirmation of statistically significant links between dry events and the precursor mechanisms, processes that modulate their trajectories, and also their impacts on rainfall. All three of these links are potentially more visible on finer timescales, so will need further analysis beyond what has been achieved here. Case study analysis will reveal the finer details on what controls dry event occurrence, and impacts on convection and rainfall over the Maritime Continent. Future work may also involve repeating the presented analysis, but for other regions of the Maritime Continent.

Impacts originating from both the abrupt pauses in convection, enabling recharge in boundary layer moisture, and also enhanced rainfall/steering of convection on margins through dynamical uplift and low-level interactions, are critical to understand. Future work should involve incorporation of both reanalysis and model data, as this will allow testing of the representation of synoptic processes such as dry air intrusions in global and regional simulations, while increasing our understanding of the associated mechanisms particularly over the Maritime Continent. These include interactions with the climatological mean circulation, as well as potentially large-scale modes of variability. Precise details on the influence of the MJO and whether it influences circulation and geopotential anomalies regulating dry air intrusions were not covered in this research and would require filtering of the MJO signal in relation to these events. Interactions between dry air intrusions and background modes of variability, however, may vary across the Maritime Continent, as the modes exert different controls on meteorology based on geographical location. Therefore, more generalised assumptions on their interactions over the whole of the Maritime Continent cannot be made based on what was learnt from studying the southern portion of the region.

Regardless, our work has provided insight into key processes and impacts linked to dry air intrusions (in terms of both rainfall suppression and enhancement), supporting and expanding on past studies. Improving our general understanding of Maritime Continent precipitation patterns will provide benefits for forecasting and issuing severe weather warnings, as well as validation of numerical weather prediction models. Any improvements to regional systematic biases and our understanding of more complex processes too will ultimately contribute to improved situational

1 awareness for local agencies, decision makers, and communities.

## 2 Acknowledgements

3 We wish to thank John Marsham, Amanda Maycock, and researchers involved in the TerraMaris project for their input.  
 4 We also wish to thank the reviewers for their constructive feedback on our manuscript. ERA5 reanalysis data was  
 5 obtained from the Copernicus Climate Data Store through <https://cds.climate.copernicus.eu>. GPM rainfall data was  
 6 available as a pre-processed product which had used the IMERG V06 algorithm (Huffman et al., 2020) as highlighted in  
 7 the Methods. Monthly ENSO ONI data was made available through the NOAA National Weather Service Climate Pre-  
 8 diction Center's website through <https://origin.cpc.ncep.noaa.gov>. Monthly IOD DMI data was accessed through the  
 9 NOAA Earth System Research Laboratories Physical Sciences Laboratory's website on <https://psl.noaa.gov>. Daily MJO  
 10 RMM data as per the methodology of Wheeler and Hendon (2004) were downloaded from <http://www.bom.gov.au/climate/mjo>.

## 11 References

- 12 Allen, G., Vaughan, G., Brunner, D., May, P. T., Heyes, W., Minnis, P. and Ayers, J. K. (2009), 'Modulation of tropical convection  
 13 by breaking Rossby waves', Quarterly Journal of the Royal Meteorological Society **135**, 125–137.
- 14 Appenzeller, C. and Davies, H. (1992), 'Structure of stratospheric intrusions into the troposphere', Nature **358**, 570–572.
- 15 Berry, G. J. and Reeder, M. J. (2016), 'The dynamics of Australian monsoon bursts', Journal of the Atmospheric Sciences  
 16 **73**, 55–69.
- 17 Birch, C. E., Webster, S., Peatman, S. C., Parker, D. J., Matthews, A. J., Li, Y. and Hassim, M. E. (2016), 'Scale interactions  
 18 between the MJO and the western Maritime Continent', Journal of Climate **29**, 2471–2492.
- 19 Pithell, M., Gray, L. J. and Cox, B. D. (1999), 'A Three-Dimensional View of the Evolution of Midlatitude Stratospheric Intru-  
 20 sions', Journal of the Atmospheric Sciences **56**, 673–688.
- 21 Brown, R. G. and Zhang, C. (1997), 'Variability of Midtropospheric Moisture and Its Effect on Cloud-Top Height Distribution  
 22 during TOGA COARE', Journal of the Atmospheric Sciences **54**, 2760–2774.
- 23 Browning, K. A. (1997), 'The dry intrusion perspective of extra-tropical cyclone development', Meteorological Applications  
 24 **4**, 317–324.
- 25 Casey, S. P. F., Dessler, A. E. and Schumacher, C. (2009), 'Five-year Climatology of Midtroposphere Dry Air Layers in Warm  
 26 Tropical Ocean Regions as viewed by AIRS/Aqua', Journal of Applied Meteorology and Climatology **48**, 1831–1842.
- 27 Chen, S. S., Kerns, B. W., Guy, N., Jorgensen, D. P., Delanoë, J., Viltard, N., Zappa, C. J., Judt, F., Lee, C. Y. and Savarin, A. (2016),  
 28 'Aircraft Observations of Dry Air, the ITCZ, Convective Cloud Systems, and Cold Pools in MJO during DYNAMO', Bulletin  
 of the American Meteorological Society **97**, 405–423.
- 29 Danielsen, E. F. (1968), 'Stratospheric-Tropospheric Exchange Based on Radioactivity, Ozone and Potential Vorticity', Journal  
 30 of the Atmospheric Sciences **25**, 502–518.
- 31 Vries, A. J., Feldstein, S. B., Riemer, M., Tyrllis, E., Sprenger, M., Baumgart, M., Fnais, M. and Lelieveld, J. (2016), 'Dynamics of  
 32 tropical-extratropical interactions and extreme precipitation events in Saudi Arabia in autumn, winter and spring', Quarterly  
 33 Journal of the Royal Meteorological Society **142**, 1862–1880.
- 34 de Vries, A. J., Ouwensloot, H. G., Feldstein, S. B., Riemer, M., Kenawy, A. M. E., McCabe, M. F. and Lelieveld, J. (2018), 'Iden-  
 35 tification of Tropical-Extratropical Interactions and Extreme Precipitation Events in the Middle East Based On Potential  
 36 Vorticity and Moisture Transport', Journal of Geophysical Research: Atmospheres **123**, 861–881.

- 1 Draxler, R. R., Spring, S., Maryland, U. S. A. and Hess, G. D. (1998), 'An Overview of the HYSPLIT\_4 Modelling System for  
2 Trajectories, Dispersion, and Deposition', Australian Meteorological Magazine **47**, 295–308.
- 3 Feng, L., Zhang, T., Koh, T. Y. and Hill, E. M. (2021), 'Selected Years of Monsoon Variations and Extratropical Dry-Air Intrusions  
4 Compared with the Sumatran GPS Array Observations in Indonesia', Journal of the Meteorological Society of Japan  
5 **99**, 505–536.
- 6 Ferrett, S., Yang, G. Y., Woolnough, S. J., Methven, J., Hodges, K. and Holloway, C. E. (2020), 'Linking extreme precipitation in  
7 Southeast Asia to equatorial waves', Quarterly Journal of the Royal Meteorological Society **146**, 665–684.
- 8 Fletcher, J. K., Parker, D. J., Hunt, K. M., Vishwanathan, G. and Govindankutty, M. (2018), 'The interaction of Indian monsoon  
9 depressions with northwesterly midlevel dry intrusions', Monthly Weather Review **146**, 679–693.
- 10 Fletcher, J. K., Parker, D. J., Turner, A. G., Menon, A., Martin, G. M., Birch, C. E., Mitra, A. K., Mrudula, G., Hunt, K. M., Taylor,  
11 C. M., Houze, R. A., Brodzik, S. R. and Bhat, G. S. (2020), 'The dynamic and thermodynamic structure of the monsoon  
12 over southern India: New observations from the INCOMPASS IOP', Quarterly Journal of the Royal Meteorological Society  
13 **146**, 2867–2890.
- 14 Yanagisaki, B. M. and Waugh, D. W. (2008), 'Connections between potential vorticity intrusions and convection in the eastern  
15 tropical Pacific', Journal of the Atmospheric Sciences **65**, 987–1002.
- 16 Gill, A. (1980), 'Some simple solutions for heat-induced tropical circulation', Quart. J. R. Met. Soc **106**, 447–462.
- 17 Nylock, M. and McBride, J. (2001), 'Spatial Coherence and Predictability of Indonesian Wet Season Rainfall', Journal of  
18 Climate **14**, 3882–3887.
- 19 Hendon, H. H. and Salby, M. L. (1994), 'The Life Cycle of the Madden–Julian Oscillation', American Meteorological Society  
20 **51**, 2225–2237.
- 21 Hersbach, H., Bell, B., Berrisford, P., Hirahara, S., Horányi, A., Muñoz-Sabater, J., Nicolas, J., Peubey, C., Radu, R., Schepers,  
22 D., Simmons, A., Soci, C., Abdalla, S., Abellan, X., Balsamo, G., Bechtold, P., Biavati, G., Bidlot, J., Bonavita, M., Chiara,  
23 G. D., Dahlgren, P., Dee, D., Diamantakis, M., Dragani, R., Flemming, J., Forbes, R., Fuentes, M., Geer, A., Haimberger,  
24 L., Healy, S., Hogan, R. J., Hólm, E., Janisková, M., Keeley, S., Laloyaux, P., Lopez, P., Lupu, C., Radnoti, G., de Rosnay, P.,  
25 Rozum, I., Vamborg, F., Villaume, S. and Thépaut, J. N. (2020), 'The ERA5 global reanalysis', Quarterly Journal of the Royal  
26 Meteorological Society **146**, 1999–2049.
- 27 Homeyer, C. R. and Bowman, K. P. (2013), 'Rossby wave breaking and transport between the tropics and extratropics above  
28 the subtropical jet', Journal of the Atmospheric Sciences **70**, 607–626.
- 29 Huffman, G. J., Bolvin, D. T., Braithwaite, D., Hsu, K., Joyce, R., Kidd, C., Nelkin, E. J., Sorooshian, S., Tan, J. and Xie, P.  
30 (2020), 'Nasa Global Precipitation Measurement (GPM) Integrated Multi-satellite Retrievals for GPM (IMERG): Algorithm  
31 Theoretical Basis Document (ATBD) Version 06'.  
32 URL: [https://gpm.nasa.gov/sites/default/files/document\\_files/IMERG\\_ATBD\\_V06.pdf](https://gpm.nasa.gov/sites/default/files/document_files/IMERG_ATBD_V06.pdf)
- 33 Ichikawa, H. and Yasunari, T. (2006), 'Time-Space Characteristics of Diurnal Rainfall over Borneo and Surrounding Oceans as  
34 Observed by TRMM-PR', Journal of Climate **19**, 1238–1260.
- 35 Jin, F. and Hoskins, B. J. (1995), 'The Direct Response to Tropical Heating in a Baroclinic Atmosphere', Journal of the  
36 Atmospheric Sciences **52**, 307–319.
- 37 Johnson, R. H., Ciesielski, P. E. and Cotturone, J. A. (2001), 'Multiscale Variability of the Atmospheric Mixed Layer over the  
38 Western Pacific Warm Pool', Journal of the Atmospheric Sciences **58**, 2729–2750.
- 39 Kerns, B. W. and Chen, S. S. (2014), 'Equatorial dry air intrusion and related synoptic variability in MJO initiation during  
40 DYNAMO', Monthly Weather Review **142**, 1326–1343.



- 1 Knippertz, P. (2007), 'Tropical-extratropical interactions related to upper-level troughs at low latitudes', Dynamics of  
 2 Atmospheres and Oceans **43**, 36–62.
- 3 Kumar, K. N., Phanikumar, D. V., Sharma, S., Basha, G., Naja, M., Ouarda, T. B., Ratnam, M. V. and kumar, K. K. (2019), 'Influence  
 4 of tropical-extratropical interactions on the dynamics of extreme rainfall event: A case study from Indian region', Dynamics  
 5 of Atmospheres and Oceans **85**, 28–40.
- 6 Kuznetsova, D., Dauhut, T. and Chaboureau, J. P. (2019), 'The Three Atmospheric Circulations over the Indian Ocean and the  
 7 Maritime Continent and Their Modulation by the Passage of the MJO', Journal of the Atmospheric Sciences **76**, 517–531.
- 8 Lucas, C. and Zipser, E. J. (2000), 'Environmental Variability during TOGA COARE', Journal of the Atmospheric Sciences  
 9 **57**, 2333–2350.
- 10 Lucas, C., Zipser, E. J. and Ferrier, B. S. (2000), 'Sensitivity of Tropical West Pacific Oceanic Squall Lines to Tropospheric Wind  
 11 and Moisture Profiles', Journal of the Atmospheric Sciences **57**, 2351–2373.
- 12 Madden, R. A. and Julian, P. R. (1971), 'Detection of a 40–50 Day Oscillation in the Zonal Wind in the Tropical Pacific', Journal  
 13 of the Atmospheric Sciences **28**, 702–708.
- 14 Madden, R. A. and Julian, P. R. (1972), 'Description of Global-Scale Circulation Cells in the Tropics with a 40–50 Day Period',  
 15 Journal of the Atmospheric Sciences **29**, 1109–1123.
- 16 Madden, R. A. and Julian, P. R. (1994), 'Observations of the 40–50-Day Tropical Oscillation – A Review', Monthly Weather  
 17 Review **122**, 814–837.
- 18 Maloney, E. D. and Hartmann, D. L. (1998), 'Frictional Moisture Convergence in a Composite Life Cycle of the Madden-Julian  
 19 Oscillation', Journal of Climate **11**, 2387–2403.
- 20 Mapes, B. E. and Zuidema, P. (1996), 'Radiative-Dynamical Consequences of Dry Tongues in the Tropical Troposphere', Journal  
 21 of the Atmospheric Sciences **53**, 620–638.
- 22 Matsuno, T. (1966), 'Quasi-Geostrophic Motions in the Equatorial Area\*', Journal of the Meteorological Society of Japan  
 23 **44**, 25–43.
- 24 Matthews, A. J. (2000), 'Propagation mechanisms for the Madden-Julian Oscillation', Q. J. R. Meteorol. Soc. **126**, 2637–2651.
- 25 Mori, S., Hamada, J.-I., Yamanaka, M. D., Okamoto, N., Murata, F., Sakurai, N. and Hashiguchi, H. (2004), 'Diurnal Land-Sea  
 26 Rainfall Peak Migration over Sumatera Island, Indonesian Maritime Continent, Observed by TRMM Satellite and Intensive  
 27 Rawinsonde Soundings', Monthly Weather Review **132**, 2021–2039.
- 28 Murata, F., Yamanaka, M. D., Mori, S., Kudsy, M., Sribimawati, T. and Suhardi, B. (2006), 'Dry Intrusions Following Eastward-  
 29 Propagating Synoptic-Scale Cloud Systems over Sumatera Island', Journal of the Meteorological Society of Japan **84**, 277–  
 30 294.
- 31 Narulita, I. and Ningrum, W. (2018), 'Extreme flood event analysis in Indonesia based on rainfall intensity and recharge capac-  
 32 ity', IOP Conference Series: Earth and Environmental Science **118**.
- 33 Neale, R. and Slingo, J. (2003), 'The Maritime Continent and Its Role in the Global Climate: A GCM Study', Journal of Climate  
 34 **16**, 834–848.
- 35 NOAA (2019), 'El Niño regions'.  
 36 **URL:** [https://www.cpc.ncep.noaa.gov/products/analysis\\_monitoring/ensostuff/nino\\_regions.shtml](https://www.cpc.ncep.noaa.gov/products/analysis_monitoring/ensostuff/nino_regions.shtml)
- 37 Numaguti, A. (1995), 'Characteristics of 4-to-20-Day-Period Disturbances Observed in the Equatorial Pacific during the TOGA  
 38 COARE IOP', Journal of the Meteorological Society of Japan **73**, 353–377.

- 1 Parker, D. J., Willetts, P., Birch, C., Turner, A. G., Marsham, J. H., Taylor, C. M., Kolusu, S. and Martin, G. M. (2016), 'The  
2 interaction of moist convection and mid-level dry air in the advance of the onset of the Indian monsoon', Quarterly Journal  
3 of the Royal Meteorological Society **142**, 2256–2272.
- 4 Parsons, D. B., Yoneyama, K. and Redelsperger, J.-L. (2000), 'The evolution of the tropical western Pacific atmosphere-ocean  
5 system following the arrival of a dry intrusion', Q. J. R. Meteorol. Soc **126**, 517–548.
- 6 Peatman, S. C., Matthews, A. J. and Stevens, D. P. (2014), 'Propagation of the Madden-Julian Oscillation through the Maritime  
7 Continent and scale interaction with the diurnal cycle of precipitation', Quarterly Journal of the Royal Meteorological  
8 Society **140**, 814–825.
- 9 Peatman, S. C., Schwendike, J., Birch, C. E., Marsham, J. H., Matthews, A. J. and Yang, G.-Y. (2021), 'A local-to-large scale view  
10 of Maritime Continent rainfall: control by ENSO, MJO and equatorial waves', Journal of Climate **34**, 8933–8953.
- 11 Pohl, B., Fauchereau, N., Richard, Y., Rouault, M. and Reason, C. J. (2009), 'Interactions between synoptic, intraseasonal and  
12 interannual convective variability over Southern Africa', Climate Dynamics **33**, 1033–1050.
- 13 Qian, J. H. (2008), 'Why Precipitation Is Mostly Concentrated over Islands in the Maritime Continent', Journal of the  
14 Atmospheric Sciences **65**, 1428–1441.
- 15 Ramage, C. S. (1968), 'Role of a Tropical "Maritime Continent" in the Atmospheric Circulation', Monthly Weather Review  
16 **96**, 365–370.
- 17 Ranjani, S. P. and Walsh, K. J. (2013), 'Influence of ENSO on the diurnal cycle of rainfall over the Maritime Continent and  
18 Australia', Journal of Climate **26**, 1304–1321.
- 19 Raveh-Rubin, S. (2017), 'Dry intrusions: Lagrangian climatology and dynamical impact on the planetary boundary layer', Journal  
20 of Climate **30**, 6661–6682.
- 21 Redelsperger, J.-L., Parsons, D. B. and Guichard, F. (2002), 'Recovery Processes and Factors Limiting Cloud-Top Height follow-  
22 ing the Arrival of a Dry Intrusion Observed during TOGA COARE', Journal of the Atmospheric Sciences **59**, 2438–2457.
- 23 Rodwell, M. J. (1997), 'Breaks in the Asian Monsoon: The Influence of Southern Hemisphere Weather Systems', Journal of  
24 the Atmospheric Sciences **54**, 2597–2611.
- 25 Ryoo, J.-M., Waugh, D. W. and Gettelman, A. (2008), 'Variability of subtropical upper tropospheric humidity', Atmos. Chem.  
26 Phys **8**, 2643–2655.
- 27 Saji, N., Goswami, B., Vinayachandran, P. and Yamagata, T. (1999), 'A dipole mode in the tropical Indian Ocean', Nature  
28 **401**, 360–363.
- 29 Saji, N. and Yamagata, T. (2003), 'Possible impacts of Indian Ocean Dipole mode events on global climate', Climate Research  
30 **25**, 151–169.
- 31 Seto, T. H., Yamamoto, M. K., Hashiguchi, H., Fukao, S., Abo, M., Kozu, T. and Kudsy, M. (2006), 'Observational Study on  
32 Westerly Wind Burst over Sumatra, Indonesia by the Equatorial Atmosphere Radar - A Case Study During the First CPEA  
33 Campaign', Journal of the Meteorological Society of Japan **84A**, 95–112.
- 34 Silverman, V., Nahum, S. and Raveh-Rubin, S. (2021), 'Predicting origins of coherent air mass trajectories using a neural net-  
35 work—the case of dry intrusions', Meteorological Applications **28**.
- 36 Stohl, A. (2001), 'A 1-year Lagrangian "climatology" of airstreams in the Northern Hemisphere troposphere and lowermost  
37 stratosphere', Journal of Geophysical Research Atmospheres **106**, 7263–7279.
- 38 Tompkins, A. M. (2001), 'Organization of Tropical Convection in Low Vertical Wind Shears: The Role of Water Vapor', Journal  
39 of the Atmospheric Sciences **58**, 529–545.

- 1 van der Wiel, K., Matthews, A. J., Stevens, D. P. and Joshi, M. M. (2015), 'A dynamical framework for the origin of the diagonal  
2 South Pacific and South Atlantic Convergence Zones', Quarterly Journal of the Royal Meteorological Society **141**, 1997–  
3 2010.
- 4 Vaughan, G., Antonescu, B., Schultz, D. M. and Dearden, C. (2017), 'Invigoration and capping of a convective rainband ahead  
5 of a potential vorticity anomaly', Monthly Weather Review **145**, 2093–2117.
- 6 Vincent, C. L. and Lane, T. P. (2016), 'Evolution of the diurnal precipitation cycle with the passage of a Madden-Julian oscillation  
7 event through the Maritime Continent', Monthly Weather Review **144**, 1983–2005.
- 8 Volonté, A., Turner, A. G. and Menon, A. (2020), 'Air mass analysis of the processes driving the progression of the Indian  
9 summer monsoon', Quarterly Journal of the Royal Meteorological Society **146**, 2949–2980.
- 10 Wang, S., Sobel, A. H., Zhang, F., Sun, Y. Q., Yue, Y. and Zhou, L. (2015), 'Regional Simulation of the October and Novem-  
11 ber MJO Events Observed during the CINDY/DYNAMO Field Campaign at Gray Zone Resolution', Journal of Climate  
12 **28**, 2097–2119.
- 13 Ward, N., Fink, A. H., Keane, R. J., Guichard, F., Marsham, J. H., Parker, D. J. and Taylor, C. M. (2021), 'Synoptic timescale  
14 linkage between midlatitude winter troughs Sahara temperature patterns and northern Congo rainfall: A building block of  
15 regional climate variability', International Journal of Climatology **41**, 3153–3173.
- 16 Waugh, D. W. and Polvani, L. M. (2000), 'Climatology of intrusions into the tropical upper troposphere', Geophysical Research  
17 Letters **27**, 3857–3860.
- 18 Wernli, H. and Davies, H. C. (1997), 'A Lagrangian-based analysis of extratropical cyclones. I: The method and some applica-  
19 tions', Quarterly Journal of the Royal Meteorological Society **123**, 467–489.
- 20 Wheeler, M. C. and Hendon, H. H. (2004), 'An All-Season Real-Time Multivariate MJO Index: Development of an Index for  
21 Monitoring and Prediction', Monthly Weather Review **132**, 1917–1932.
- 22 Wheeler, M. and Kiladis, G. N. (1999), 'Convectively coupled equatorial waves: Analysis of clouds and temperature in the  
23 wavenumber-frequency domain', Journal of the Atmospheric Sciences **56**, 374–399.
- 24 Wijayanti, P., Zhu, X., Hellegers, P., Budiyo, Y. and van Ierland, E. C. (2017), 'Estimation of river flood damages in Jakarta,  
25 Indonesia', Natural Hazards **86**, 1059–1079.
- 26 Yamanaka, M. D., Ogino, S. Y., Wu, P. M., Hamada, J.-I., Mori, S., Matsumoto, J. and Syamsudin, F. (2018), 'Maritime Continent  
27 coastlines controlling Earth's climate', Progress in Earth and Planetary Science **5**.
- 28 Yang, G.-Y., Hoskins, B. and Slingo, J. (2003), 'Convectively Coupled Equatorial Waves: A New Methodology for Identifying  
29 Wave Structures in Observational Data', Journal of the Atmospheric Sciences **60**, 1637–1654.
- 30 Yang, G.-Y. and Slingo, J. (2001), 'The Diurnal Cycle in the Tropics', Monthly Weather Review **129**, 784–801.
- 31 Yang, S., Cui, X. and Ran, L. (2009), 'Analyses of Dry Intrusion and Instability during a Heavy Rainfall Event that Occurred in  
32 Northern China', Atmospheric and Oceanic Science Letters **2**, 108–112.
- 33 Yokoi, S., Mori, S., Katsumata, M., Geng, B., Yasunaga, K., Syamsudin, F., Nurhayati and Yoneyama, K. (2017), 'Diurnal cycle of  
34 precipitation observed in the western coastal area of Sumatra Island: Offshore preconditioning by gravity waves', Monthly  
35 Weather Review **145**, 3745–3761.
- 36 Yoneyama, K. and Fujitani, T. (1995), 'The Behavior of Dry Westerly Air Associated With Convection Observed during the  
37 TOGA-COARE R/V Natsushima Cruise', Journal of the Meteorological Society of Japan **73**, 291–304.
- 38 Yoneyama, K. and Parsons, D. B. (1999), 'A Proposed Mechanism for the Intrusion of Dry Air into the Tropical Western Pacific  
39 Region', Journal of the Atmospheric Sciences **56**, 1524–1546.
- 40 Zhang, C. and Chou, M.-D. (1999), 'Variability of Water Vapor, Infrared Radiative Cooling, and Atmospheric Instability for  
41 Deep Convection in the Equatorial Western Pacific', Journal of the Atmospheric Sciences **56**, 711–723.